Direct Imaging of Self-Organized Comb Copolymer-like Systems Obtained by Hydrogen Bonding: Poly(4-vinylpyridine)−4-Nonadecylphenol

J. Ruokolainen, J. Tanner, and O. Ikkala*

Department of Engineering Physics and Mathematics, Helsinki University of Technology, P.O. Box 2200, FIN-02015 HUT, Espoo, Finland

G. ten Brinke*,†

Department of Polymer Science and Materials Science Center, University of Groningen, Nijenborgh 4, 9747 AG Groningen, The Netherlands

E. L. Thomas

Department of Materials Science & Engineering, Massachusetts Institute of Technology, Cambridge, Massachusetts 02139

Received December 2, 1997; Revised Manuscript Received March 16, 1998

ABSTRACT: Comb copolymer-like systems obtained by hydrogen bonding between flexible polymers and nonmesogenic amphiphiles represent a class of supramolecular materials with interesting self-organizing properties. Here we present the first results of transmission electron microscopy applied to mesomorphic systems of poly(4-vinyl pyridine)−4-nonadecylphenol as a characteristic example. Phase contrast imaging of iodine-stained samples confirms the highly ordered lamellar structures with a long period of around 40 Å inferred also from small-angle X-ray scattering data.

1. Introduction

Comb copolymer-like molecules obtained by hydrogen bonding between flexible polymers (noncharged or charged) and nonmesogenic amphiphiles represent a new class of supramolecular materials exhibiting a very rich phase behavior. Within this concept, particularly illustrative model systems have shown to be poly(4-vinylpyridine) (P4VP) and poly(4-vinylpyridinium sulfonates) where oligomeric amphiphiles are hydrogen-bonded.[1−9] Related work on hydrogen bonded supramolecular polymer structures has been published emphasizing various aspects of the formation of mesomorphic order,[10,11] liquid crystallinity using mesogenic amphiphiles,[12−15] and liquid crystalline hydrogen-bonded networks.[16]

From the various nonmesogenic amphiphiles investigated so far, the alkylphenols appeared to be the most interesting and versatile with respect to nanostructure formation.[5] It has been shown that the phase behavior can be tailored to a large extent by balancing the competing attractive and repulsive interactions. In the case of alkylphenols, the hydrogen bonding to P4VP is strong and the phase behavior is dominated by the repulsion between the alkyl side chains and the polar backbone. Stronger repulsion can be obtained by longer alkyl side chains but, interestingly, also by adjusting the polarity of the polymer by introducing charges. The most recent example is P4VP quaternized using sulfonic acids such as CH_3SO_3H. The quaternization results in poly(4-vinylpyridinium methanesulfonate) and the sulfonate groups, in turn, act as hydrogen-bonding acceptors for the alkylphenols.[2,17]

Depending on the balance between the repulsive and attractive interactions, a sequence of phase transitions can occur. Assuming the hydrogen bonding to be sufficiently strong, a well-ordered microphase-separated structure is found near room temperature. When the temperature is raised, an order−disorder transition (ODT) will usually take place but its temperature varies widely depending on the repulsive interaction. Further heating will ultimately lead to breaking of most of the hydrogen bonds since they are highly directionally specific and thus entropically unfavorable. Then the repulsive interactions dominate, which might result in macrophase separation. As is quite common for systems involving hydrogen bonds, this macrophase separation is in the form of a closed loop because at still higher temperatures the entropy of mixing will dominate.[18]

It is believed that new technologies could be based on the sophisticated use of self-organized materials.[19] The ordered structures of our samples are of special interest in this respect because of their simple and straightforward way of preparation. Recent theoretical investigation into the nature of the phase behavior and microphase-separated structures of such systems demonstrated that the familiar lamellar, hexagonal cylinder, and bcc sphere structures can all be observed but that the reversible nature of the bonding makes the phase diagram far more complicated than for the familiar (di)-block copolymer systems.[20,21] Experimentally, we have investigated the structure formation mainly by small-angle X-ray scattering (SAXS)[3,4,6] supported by dynamic mechanical spectroscopy.[6] Most of the systems considered exhibited an ODT manifested by a distinct scattering pattern. Despite the variety of systems used so far, the SAXS data indicate that only lamellar structures are present with long periods on the order of 30−50 Å, consisting of alternating alkyl and polar backbone layers. If the alkyl side chains are sufficiently long, they will crystallize at or above room temperature. To image

† Also Helsinki University of Technology.

S0024-9297(97)01747-6 CCC: $15.00
Published on Web 05/15/1998

these structures by transmission electron microscopy, we synthesized an alkylphenol with a somewhat longer alkyl tail than the pentadecyl group used in our previous studies, i.e., 4-nonadecylphenol (NDP). As will be shown, this raises the ODT from 60 to about 100 °C, whereas the crystallization sets in already at approximately 55 °C, leading to a crystalline alkyl layer at room temperature. With this system we were able to obtain the first transmission electron microscopy (TEM) micrographs confirming the highly ordered lamellar structure for the nominally fully complexed system of P4VP−$NDP_{1.0}$; i.e., the system contains equal numbers of pyridine and phenol groups. In conjunction with TEM, SAXS and Fourier transform infrared (FTIR) data are presented to corroborate the analysis.

2. Experimental Section

Materials. Atactic P4VP with a viscosity-averaged molecular weight of M_v = 49 000 was acquired from Polysciences Ltd. and was used without further purification. The synthesis and characterization of 4-nonadecylphenol is described in the Appendix.

Sample Preparation. Both P4VP and NDP were first dried in a vacuum at 60 °C for at least 24 h. P4VP−$NDP_{1.0}$ complexes were prepared by dissolving both compounds in analysis grade dichloromethane first dried using 3 Å molecular sieves. Dichloromethane and NDP were mixed together until a clear solution was obtained. P4VP was then added, followed by mechanical stirring at room temperature. The concentration of polymer in the solvent was kept low (less than 1 wt %) to ensure homogeneous complex formation. Subsequently, the solvent was evaporated on a hot plate at 50 °C. The final drying took place in a vacuum at 60 °C for ca. 2 days, and the samples were then stored in a desiccator.

Bulk samples for TEM characterization were first annealed at about 30 deg above the ODT temperature for 15 min followed by a slow cooling to room temperature. The samples were embedded in epoxy and cured at 60 °C overnight. Ultrathin sections were cut from the embedded bulk specimen using a Reichert Ultracut E ultramicrotome and a diamond knife at room temperature. The resulting sections were approximately 30−40 nm thick, as judged from the light gray color. Sections were picked up on 600 mesh copper grids and, to enhance contrast, the microtomed sections were stained in the vapor of I_2 crystals. Some of the stained samples were carbon coated in a vacuum evaporator in order to enhance the stability in the beam.

Small-Angle X-ray Scattering. The small-angle X-ray scattering was performed at the DESY/HASYLAB synchrotron source in Hamburg, Germany, using the Polymer Beamline. Details on the instrumentation can be found in ref 22.

Infrared Spectroscopy. Infrared spectra were obtained using a Nicolet 730 FTIR spectrometer. Samples were prepared by melting the sample directly onto potassium bromide crystals. To prevent any evaporation of 4-nonadecylphenol, an additional KBr layer was compressed on top of the sample to achieve a sealed sample.

Electron Microscopy. Bright field TEM was performed on either a JEOL-1200EX or a JEOL-2000FX transmission electron microscope with a tungsten filament and a LaB_6 source. Microscopes were operated at accelerating voltages of 60 and 100 kV, respectively.

3. Results

The hydrogen bonding between 3-pentadecylphenol and P4VP is rather strong, and at not too high a temperature equal numbers of pyridine and phenol groups lead to nearly fully complexed comb copolymer-like systems.[3] Figure 1 shows the repeat unit of P4VP−$NDP_{1.0}$, involving the somewhat longer 4-nonadecylphenol, assuming full complexation (P4VP−NDP_x denotes a mixture of poly(4-vinylpyridine) and 4-nonadecylphenol with x NDP molecules per repeat unit of P4VP). Hydrogen bonding is a directionally specific interaction, and the combination of energy gain with entropy loss upon formation implies that the number of hydrogen bonds might decrease considerably upon even a relatively small temperature increase.[20] This property is directly related to the phenomenon of reappearing phases.[18,20,21] To investigate the temperature dependence of the hydrogen bonding in P4VP−$NDP_{1.0}$, FTIR spectra were recorded as a function of temperature. FTIR permits the study of the state of the hydrogen-bonding acceptor moiety,[3] i.e., whether the pyridine group is free (993 cm^{-1}) or hydrogen bonded (1003 cm^{-1}). Figure 2 presents the FTIR spectra as a function of temperature for this region. It demonstrates that at room temperature most, but not all, pyridine groups are hydrogen bonded. Furthermore, the fraction of free pyridine groups increases gradually as a function of temperature and, for example, at 120 °C a considerable amount of the pyridine groups are "free". Therefore, in P4VP−$NPD_{1.0}$ the fraction of the non-hydrogen-bonded pyridine groups is larger than in the corresponding complex using pentadecylphenol, as could be expected from the longer repulsive alkyl tail.

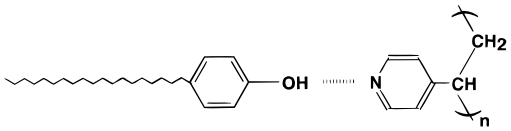

Figure 1. Schematics of hydrogen bonding between poly(4-vinylpyridine) and 4-nonadecylphenol.

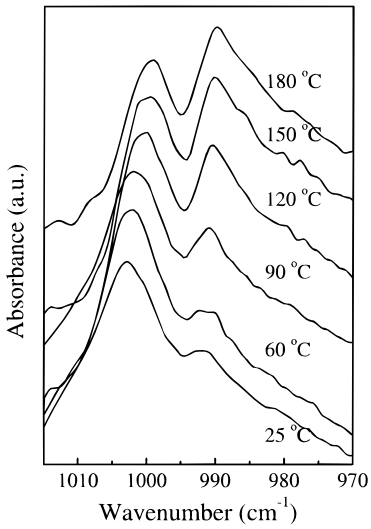

Figure 2. FTIR absorption bands at different temperatures showing the characteristic free and hydrogen-bonded pyridine bands at about 993 and 1003 cm^{-1}.

Figure 3 presents the SAXS data for P4VP−$NDP_{1.0}$ as a function of temperature. As is expected, the same features observed previously for P4VP−pentadecylphenol are also present here.[4] At elevated temperatures the system is in a homogeneous state with a characteristic correlation hole scattering peak. The appearance of a distinct correlation hole peak is evidence for the presence of many hydrogen bonds.[23] During cooling at 20 °C/min, an order−disorder transition (ODT) occurs at 90 °C, manifested by a strong increase in the scattering peak height and a corresponding decrease in width. Due to the relatively high scanning rate, the undercooling is considerable and upon heating with the

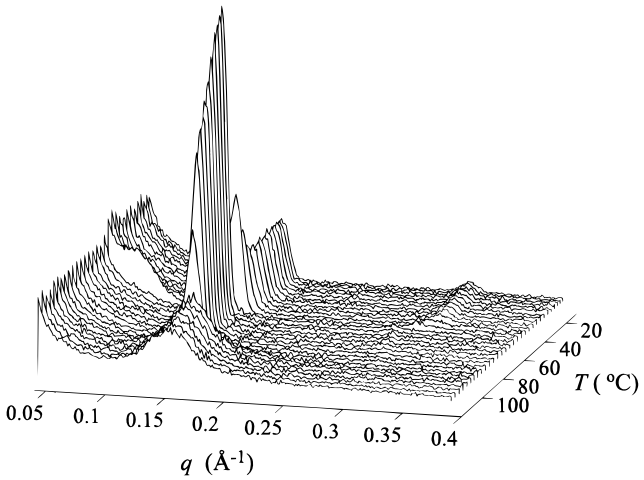

Figure 3. SAXS intensity patterns of P4VP−$NPD_{1.0}$ during cooling at 20 °C/min.

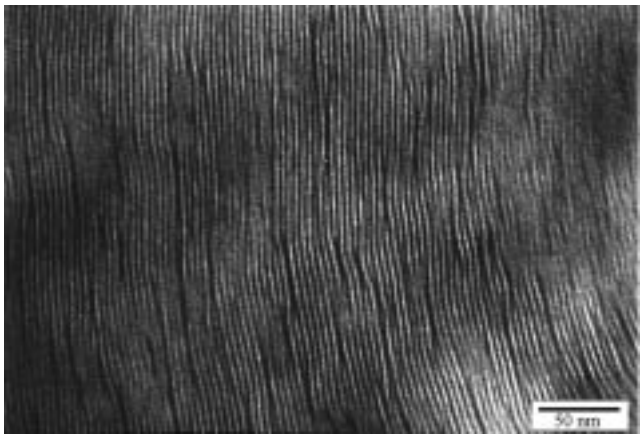

Figure 4. TEM micrograph of P4VP−$NPD_{1.0}$ illustrating the lamellar structure with a long period of ca. 40 Å.

same rate, the ODT is observed around 110 °C. Since, the ODT in the corresponding P4VP−pentadecylphenol samples occurred around 60 °C,[4] the increase in the repulsive interaction due to the increase in alkyl tail length from 15 to 19 methyl units results in an increase of approximately 40 °C in the microphase separation temperature. The SAXS data just below the ODT show only one pronounced scattering peak and a faint second-order peak, which is again a strong indication for a lamellar structure with a long period of 45 Å. Due to the faintness, the second-order reflection is only observable in a logarithmic presentation of the intensity. The suppression of clear even orders in the diffraction patterns is a strong indication that both phases, the alkyl layer and the polar backbone layer, are present in comparable volume fractions with symmetric interfaces.[24] Additional support for this statement comes from the results for further cooling, where an additional transition appears, which can be attributed to the crystallization of the alkyl side chains in the alkyl layers.[4] As in the case of pentadecylphenol, a second-order peak at twice the scattering vector of the primary peak is distinctly present, demonstrating conclusively that the ordered state consists of a lamellar morphology. Due to the better packing from crystallization, the long period decreases by approximately 4 to 41 Å. Consequently, the alternating polar and alkyl layers no longer occupy similar volume fractions and although the electron density contrast is reduced at the same time, the second-order diffraction peak becomes more pronounced. Despite a large undercooling, the crystallization already occurs around 55 °C. In the corresponding pentadecylphenol sample, i.e., P4VP−$PDP_{1.0}$, the crystallization and melting transitions occur near room temperature, a fact that is believed to be responsible for some confusing interpretations of our early results.[3] The much higher crystallization temperature in P4VP−$NDP_{1.0}$, leading to alternating amorphous and highly crystalline layers at room temperature, is the main reason this particular system was selected for the first investigation with electron microscopy.

The study of comb copolymer-like systems obtained by hydrogen bonding between flexible polymers and nonmesogenic amphiphiles is of very recent date. Antonietti and co-workers investigated similar systems involving ionic interactions, i.e., polyelectrolyte−surfactant complexes[25−27] (see also the recent review[28]). Although they did not report order−disorder transitions, the systems always being in the ordered state, many interesting ordered structures were observed. We, on the other hand, concentrated on hydrogen-bonding systems and, although the phase behavior observed (order−disorder transitions, reappearing phases, etc.) is in some respects considerably richer than for the polyelectrolyte systems, the ordered structures of all systems investigated so far are lamellar, judged from

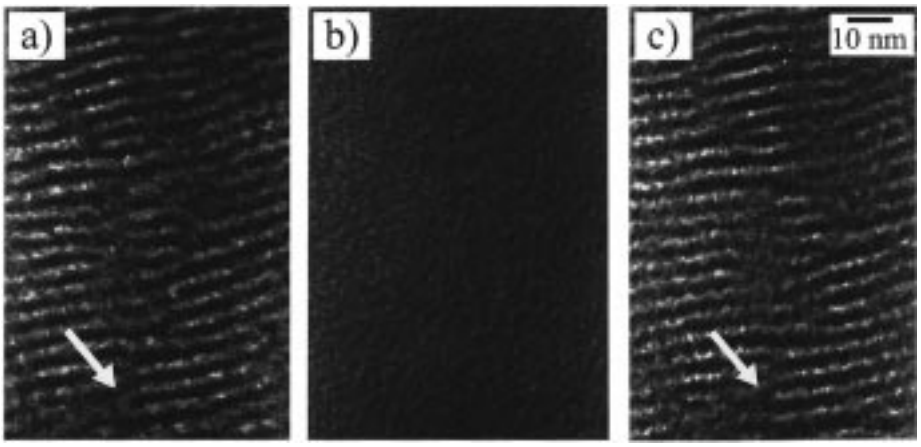

Figure 5. TEM micrograph of P4VP−$NPD_{1.0}$ at different defocus values: (a) using about −1400 nm; (b) 0 nm (in focus); (c) +1400 nm.

the SAXS data. Still, we believe that also in the hydrogen-bonded systems the sequence of structures characteristic for block copolymer systems should occur. They have already been predicted theoretically.[20] It is always revealing to have a real image of the microphase-separated structures, but the predominance of lamellar structures in our samples makes it even more important to obtain transmission electron microscopy (TEM) images.

Figure 4 shows the first transmission electron micrographs of comb copolymer-like systems obtained by hydrogen bonding. It clearly shows that P4VP−$NDP_{1.0}$ samples have lamellar or smectic structures with a characteristic period of approximately 40 Å in good agreement with the SAXS results of Figure 3. The structure contains a large number of defects, mostly in the form of edge dislocations.[29] A striking feature is the observation of the considerably thicker dark layers, corresponding to the polar layers, next to the edge dislocations. Although it is quite speculative, it seems that they represent not fully complexed P4VP polymers, which we know from the FTIR data (Figure 2) have to be present. This implies the existence of NDP rich regions as well, but it cannot be excluded that this is just in the form of additional free NDP throughout the alkyl layers (incorporated in the crystal lattice but not hydrogen bonded to a pyridine ring).

The micrograph shows P4VP−$NDP_{1.0}$ stained with I_2 vapor. Although this is the common procedure for poly(vinylpyridine)-containing polymers, in this case the situation is less clear due to the hydrogen bonding between the pyridine and phenol groups. However, since the alkyl layers are highly crystalline, the iodine vapor can only reach the polar backbone layers and the possible amorphous transition regions of the alkyl chains on the surface of the crystalline lamellae. Unlike the case of conventional P4VP-containing block copolymers, the mass density contrast created in this way still turns out to be insufficient to image the layered structures in focus.

The conventional contrast mechanism (images taken in focus) depends only on the squared amplitude of the electron wave function (mass thickness or diffraction contrast). However, in general, the image contrast also depends on the amplitude and the phase of the wave function. In optical phase contrast microscopy the changes in intensity can be obtained by using special phase contrast lenses that change uniformly the phase of selected photons. In electron microscopy, the phase shift not only depends on the mean inner potentials between different materials but also can be achieved by defocusing the microscope.[24] The optimum defocus value to image features of size $d = 1/q$, where q is a scattering vector, by using phase contrast is approximately $\Delta f = -d^2/2\lambda$. λ is the wavelength of electrons and depends on the accelerating voltage. For example, to image structures of size $d = 4.2$ nm using phase contrast with 60 kV accelerating voltage ($\lambda = 4.9$ pm), the optimum defocus value $\Delta f = -1800$ nm. When the image is "in focus", the phase contrast essentially disappears and only the mass thickness contrast contributes to the image information. Upon underfocusing, the phase contrast amplifies the mass thickness contrast and image contrast reaches the maximum. By contrast, upon overfocusing, the phase contrast is reversed and the effective contrast consists of the difference between the phase contrast and mass thickness contrast.

Figure 5 presents TEM micrographs utilizing defocus values of about −1400 nm, 0 and +1400 nm, respectively. Figure 5b has been taken approximately "in focus", and it shows hardly any contrast between the alkyl tail and the polar polymer layers despite the iodine staining. When underfocusing, the phase contrast is increased and the image contrast between different layers becomes clear; see Figure 5a. The iodine staining probably changes the mean inner potential of the polar polymer layer and therefore contributes to the phase contrast. The observation that in unstained samples the phase contrast was negligible also supports this conclusion. When overfocusing, the contrast is indeed reversed and this can be seen when parts a and c of Figure 5 are compared. To pinpoint a specific example where the reversal of the contrast can be seen clearly, the arrows in Figure 5a,c indicate a part of an edge dislocation loop with Burgers' vector $\vec{b} = 1.2$ the layer spacing. Images in Figures 5 have been taken using an accelerating voltage of 60 kV. The theoretically optimum defocus for this structure should be −1800 nm. Experimentally, the best contrast was found to be at the defocus value −1400 nm.

Considerable care has to be taken in the interpretation of phase contrast images of periodic structures obtained at large underfocus. It was demonstrated in ref 24 that the repeat period in the image is independent of defocus. However, the widths of the individual phases are a function of defocus, if the phases are not equal in size. In our case, the relatively small SAXS second-order peak intensity points toward the layer thicknesses being comparable, suggesting that this effect is minimal with this particular sample.

Summarizing, we have presented the first electron microscopy data confirming the lamellar structure in a characteristic system from the class of comb copolymer-like systems obtained by hydrogen bonding between flexible polymers and nonmesogenic amphiphiles. Future work will include further exploration of the various structures that should be realizable in these systems. Besides SAXS, TEM will remain an indispensable tool for these studies.

Acknowledgment. DESY/HASYLAB at Hamburg, Germany, is acknowledged for the beam time to perform SAXS measurements. We are grateful to Bart Jansen/DESY for assistance in the measurements. Ritva Serimaa and Mika Torkkeli of Helsinki University are acknowledged for numerous discussions on SAXS. J.R. would like to thank Len Radzilowski for useful discussions and for experimental assistance in TEM. The work has been supported by the Finnish Academy, Technology Development Centre (Finland), and Neste Foundation. This work was supported in part by the MRSEC Program of the National Science Foundation under award number DMR 94-0334. We thank the Center for Materials Science and Engineering electron microscopy facility at the Massachusetts Institute of Technology. The Department of Electron Microscopy at the Institute of Biotechnology of Helsinki University is acknowledged for the use of their facilities.

Appendix

4-*n*-Nonadecylphenol was synthesized from 1-bromooctadecane and 4-methoxybenzaldehyde by using the conventional Grignard reaction, and the product of this reaction, 1-(4-methoxyphenyl)nonadecan-1-ol, was re-

duced with hydriodic acid and red phosphorus, as described elsewhere.[30] The purification of 4-*n*-nonadecylphenol was performed by column chromatography on activated neutral alumina (Aldrich) with chloroform−ethyl acetate (98:2 vol %) as eluent.

The structure of 4-*n*-nonadecylphenol (NPD) was identified by mass spectrometry (MS), NMR, and FTIR analyses. The MS analysis was done with a VG Trio-2 quadrupole mass spectrometer by using electron impact (EI) ionization and direct insertion probe (DIP) and GCMS techniques. ^{1}H and ^{13}C spectra were recorded on a JEOL GSX-400 spectrometer operated at 400 and 100 MHz, respectively. The IR spectrum was obtained using a Nicolet 730 FTIR spectrometer.

The product gave the following IR, ^{1}H and ^{13}C NMR, and MS spectra: IR (thin film on KBr) 3354 (broad), 2952 (m), 2918 (s), 2849 (s), 1883 (w), 1615 (w), 1600 (w), 1517 (w), 1472(w), 1462 (m), 1379 (w), 1256 (w), 1111 (w), 820 (m), 720 (w), 503 (w) cm^{-1}; ^{1}H NMR (400 MHz, $CDCl_3$) $\delta = 0$ (TMS, ref), 0.88 (t, 3H, CH_3), 1.25 (s, CH_2), 1.28 (m, CH_2) (1.25 and 1.28, 32H), 1.56 (m, 2H, CH_2), 2.52 (t, 2H, CH_2), 4.59 (s, 1H, OH), 6.74 (d, 2H, ArH), 7.40 (d, 2H, ArH); ^{13}C NMR (100 MHz, $CDCl_3$) $\delta = 14.13$ (CH_3), 22.68, 29.26, 29.36, 29.52, 29.61, 29.69, 31.74, 31.92, 35.04 (CH_2), 77 ($CDCl_3$, ref) 114.98, 129.41 (arom C), 135.23 (arom quater C), 153.33 (arom C−OH); MS $m/z = 360$ (M^+, 19%), 107 ($M^+ - C_{18}H_{37}$), 100%.

References and Notes

(1) Ikkala, O.; Ruokolainen, J.; Torkkeli, M.; Serimaa, R.; ten Brinke, G. *Makromol. Chem., Macromol. Symp.* **1996**, *112*, 191.
(2) Ikkala, O.; Ruokolainen, J.; Torkkeli, M.; Tanner, J.; Serimaa, R.; ten Brinke, G. *Colloids Surf. A*, in press.
(3) Ruokolainen, J.; ten Brinke, G.; Ikkala, O.; Torkkeli, M.; Serimaa, R. *Macromolecules* **1996**, *29*, 3409.
(4) Ruokolainen, J.; Torkkeli, M.; Serimaa, R.; Komanschek, E.; Ikkala, O.; ten Brinke, G. *Phys. Rev. E* **1996**, *54*, 6646.
(5) Ruokolainen, J.; Torkkeli, M.; Serimaa, R.; Vahvaselkä, S.; Saariaho, M.; ten Brinke, G.; Ikkala, O. *Macromolecules* **1996**, *29*, 6621.
(6) Ruokolainen, J.; Torkkeli, M.; Serimaa, R.; Komanschek, B. E.; ten Brinke, G.; Ikkala, O. *Macromolecules* **1997**, *30*, 2002.
(7) ten Brinke, G.; Ruokolainen, J.; Ikkala, O. *Europhys. Lett.* **1996**, *35*, 91.
(8) ten Brinke, G.; Huh, J.; Ruokolainen, J.; Torkkeli, M.; Serimaa, R.; Ikkala, O. *Makromol. Chem., Macromol. Symp.* **1997**, *114*, 229.
(9) ten Brinke, G.; Ikkala, O. *Trends Polym. Sci.* **1997**, *5*, 213.
(10) Tal′roze, R. V.; Platé, N. A. *Polymer Sci.* **1994**, *36*, 1479.
(11) Tal′roze, R. V.; Kuptsov, S. A.; Sycheva, T. I.; Bezborodov, V. S.; Platé, N. A. *Macromolecules* **1995**, *28*, 8689.
(12) Kato, T.; Fréchet, J. M. J. *Macromolecules* **1989**, *22*, 3818.
(13) Kato, T.; Fréchet, J. M. J. *Macromolecules* **1990**, *23*, 360.
(14) Bazuin, C. G.; Tork, A. *Macromolecules* **1995**, *28*, 8877.
(15) Alder, K. I.; Stewart, D.; Imrie, C. T. *J. Mater. Chem.* **1995**, *5*, 2225.
(16) Pfaadt, M.; Moessner, G.; Pressner, D.; Valiyaveettil, S.; Boeffel, C.; Müllen, K.; Spiess, H. W. *J. Mater. Chem.* **1995**, *5*, 2195.
(17) Ruokolainen, J.; Mäkinen, R.; Torkkeli, M.; Serimaa, R.; Mäkelä, T.; ten Brinke, G.; Ikkala, O. *Science* **1998**, *280*, 557.
(18) Walker, J. S.; Vause, C. A. *Sci. Am.* **1987**, *256*, 90.
(19) Muthukumar, M.; Ober, C. K.; Thomas, E. L. *Science* **1997**, *277*, 1225.
(20) Dormidontova, E.; ten Brinke, G. *Macromolecules*, in press.
(21) Tanaka, F.; Ishida, M. *Macromolecules* **1997**, *30*, 1836.
(22) Elsner, G.; Riekel, C.; Zachmann, H. G. *Adv. Polym. Sci.* **1985**, *67*, 1.
(23) Huh, J.; Ikkala, O.; ten Brinke, G. *Macromolecules* **1997**, *30*, 1828.
(24) Handlin, D. L. J.; Thomas, E. L. *Macromolecules* **1983**, *16*, 1514.
(25) Antonietti, M.; Burger, C.; Effing, J. *Adv. Mater.* **1995**, *7*, 751.
(26) Antonietti, M.; Wenzel, A.; Thünemann, A. *Langmuir* **1996**, *12*, 2111.
(27) Antonietti, M.; Burger, C.; Thünemann, A. *Trends Polym. Sci.* **1997**, *5*, 262.
(28) Ober, C.; Wegner, G. *Adv. Mater.* **1997**, *9*, 17.
(29) Demus, D.; Richter, L. *Textures of Liquid Crystals*; Verlag Chemie; Weinheim, **1978**.
(30) Durrani, A. A.; Tyman, J. H. *J. Chem. Soc., Perkin Trans. I* **1979**, 2069.

MA971747L